Experimental Measurements of Particulate Matter Distribution in a Catalyzed Particulate Filter

Ryan Foley · John Johnson · Jeff Naber · Leigh Rogoski

Abstract The investigation of the distribution of particulate matter (PM) inside a catalyzed particulate filter (CPF) is studied in this work. The goal was to identify how loading, passive oxidation, active regeneration, and post loading conditions affect the PM distribution. The PM distribution was measured using an Advantest TAS7000 3D Imaging Analysis System, which nondestructively measures the PM distribution. A total of nine experiments were conducted, resulting in three loading scans, four passive oxidation scans, four active regeneration scans, and two post loading scans. The loading experiments were run with two different target PM loadings of 3 and 5 g/L. The passive oxidation experiments were run under two different engine conditions, and four different amounts of PM were oxidized. The active regeneration experiments were run at two target temperatures of 525 and 600 °C, and four levels of PM were oxidized. One post loading experiment was completed after a passive oxidation, and one was completed after an active regeneration. The results show that the PM distribution after loading is similar to the model-predicted PM distribution, which is calculated using the wall flow velocity distribution. The amount of PM in the substrate affects the axial distribution uniformity. The amount of PM passively oxidized or actively regenerated affects the axial distribution uniformity as well. The effect of post loading is dependent on whether the PM was passively oxidized or actively regenerated.

Abbreviations

DOC	Diesel oxidation catalyst
CPF	Catalyzed particulate filter
SCR	Selective catalytic reduction
PM	Particulate matter (includes carbonaceous and ash)
ULSD	Ultra-low sulfur diesel
IMR-MS	Ion molecule reaction mass spectrometer
SMPS	Scanning mobility particle sizer
MTU	Michigan Technological University
Baseline scan	Substrate scan taken prior to any PM loading
Axial section	One of the 64 axial planes used by the TAS7000 during substrate scanning
Axial segment	A collection of 16 or 31–32 axial sections used to describe the PM distribution
Radial section	One of the four equal area divisions in the radial plane made in each axial section
Angular increment	One of the 72 5° divisions in the angular plane made in each axial section
Quadrant	A collection of 18 angular increments used to describe the PM distribution
PR	Percentile range
UI	Uniformity index
Analysis point	The region in one angular increment, one radial section, and one axial section
Analysis area	The collection of analysis points for which the PM distribution information is calculated
Loading	Depositing PM into a CPF
	NO_2-assisted PM oxidation

R. Foley (✉)
Cummins Emission Solutions, 1801 US Hwy. 51-138, Stoughton, WI 53589, USA
e-mail: rkfoley@mtu.edu

J. Johnson · J. Naber
Michigan Technological University, 815 RL Smith Building, 1400 Townsend Drive, Houghton, MI 49931, USA

L. Rogoski
Cummins Inc., 1900 McKinley Ave., Columbus, IN 47201, USA

Passive oxidation	
Active regeneration	O_2-assisted PM oxidation
Post loading	PM loading that occurs after a passive oxidation or active regeneration
EOC	Engine operating condition

1 Introduction

Through stringent regulations, heavy-duty diesel engine emissions have been reduced throughout the world. To meet these and new regulations, the exhaust aftertreatment needs to be improved and optimized in order to reduce the fuel consumption, cost, and emissions associated with the operation of the integrated engine and aftertreatment system. A typical heavy duty aftertreatment configuration consists of a diesel oxidation catalyst (DOC), a catalyzed particulate filter (CPF), and a selective catalytic reduction (SCR) catalyst. The aftertreatment is optimized through advanced experimental measurements and development of advanced models. In particular, the operation of the CPF can be optimized through research in at least the four following areas:

1. Understanding the maximum particulate matter (PM) loading in the CPF that will not cause damage to the CPF
2. Understanding the required frequency of active regenerations to prevent nonuniform PM loading, uncontrolled regenerations, and CPF damage
3. Understanding how PM loading, active regeneration, passive oxidation, and post loading affect the PM distribution in the CPF
4. Developing high fidelity and reduced order models, validated with experimental data, that can be used for system design and control in the vehicle

High fidelity and reduced order models have the potential to be used for system design, optimization, and on-board diagnostic work. If the models are capable of predicting the PM distribution in the CPF, the frequency and duration of the active regeneration events could be optimized. Konstandopoulos, Kostoglou, and Housiada [1] showed that the PM distribution in the CPF could affect the amount of time required to remove all of the PM from the substrate. By optimizing the active regeneration strategy, based on the PM distribution, the fuel penalty associated with active regenerations could be reduced.

The optimization of the CPF is complicated due to the lack of information available on the PM distribution inside the CPF. Traditionally, measurement of the PM distribution was time intensive and resulted in destruction of the CPF. New measurement methods that utilize X-rays [2], dynamic neutron radiography [3, 4], and terahertz waves [5] enable measurement of the PM distribution CPF in three dimensions without damaging the CPF. This allows for repeated testing and more advanced analysis of the retained PM distribution.

A study was conducted to investigate the PM distribution in a CPF to determine trends for PM loading, passive oxidation, active regeneration, and post loading conditions. The study was conducted in two phases. Phase 1 was intended to develop the experimental methods and gain an initial understanding of the PM distribution. Foley, Naber, Johnson, and Rogoski presented results from the phase 1 study in reference [6], with the focus being the development of the measurement and analysis procedures. Phase 2 was an in-depth investigation into the PM distribution for carefully conducted engine experiments using previously established procedures. Foley presented an in-depth data analysis for phases 1 and 2 in reference [7]. The data collected from this study were compared with previously collected experimental data available in the literature. This work presents a literature review of previous works, a brief overview of the equipment and instrumentation used, the plan used to conduct the study, and the phase 2 results and conclusions.

Based on a review of prior work in this area, there are six ways that PM can be filtered in a wall flow device, such as a CPF. These include the following: (1) diffusion, (2) interception, (3) inertia, (4) gravity, (5) electrostatic forces, and (6) thermophoresis [8, 9]. The particle size of the PM emitted from the engine during this study was less than 1000 nm, with the peak particle size being 100 nm by number and 200 nm by volume. According to Ohara et al. [9], when the particle size of the PM is between 0 and 250 nm, diffusion is the primary filtration mechanism. Between 250 and 1000 nm, interception of the particles, or capturing the particle due to it hitting another surface, is the primary filtration mechanism. The particles will remain in the streamlines prior to contact with another surface [9]. Therefore, the profile of the wall flow velocity will affect the distribution of the PM. The modeled wall flow velocity (U_w) for three different permeability values (k_w) is shown in Fig. 1 [10]. The wall flow velocity tends to have a nearly linear profile along the length of the CPF for low permeability values. As the permeability increases, the wall flow velocity transitions to a parabolic profile. Given the particle size range in our study, it would then be expected that the measured PM distributions would have axial trends similar to the wall flow velocity distributions shown in Fig. 1.

Several studies that have either modeled PM distributions using models calibrated to simulate engine data or performed destructive PM distribution measurements. Piscaglia, Rutland, and Foster [11] give an example of the modeling work. The developed model produces an axial PM distribution similar to the axial wall flow distribution shown in Fig. 1 for a permeability value of 1.8×10^{-14} m^2. Piscaglia et al. show that the

Fig. 1 Wall flow velocity for three permeability values [10]. Reprinted from *Journal of Aerosol Science*, 40/4, Liu, Y., Gong, J., Fu, J., Cai, H., Long, G., *Nanoparticle motion trajectories and deposition in an inlet channel of wall-flow diesel particulate filter*, page 316, copyright 2008, with permission from Elsevier
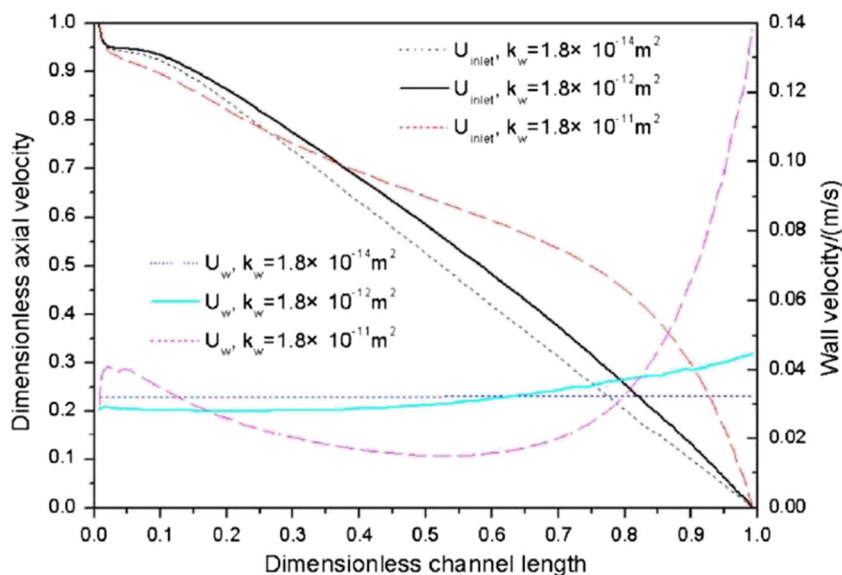
axial PM distribution is also dependent on space velocity, with higher space velocities producing a distribution with more variation.

Yi [12] developed a three-dimensional particulate filter model. The model shows that initially, the axial PM distribution follows the axial wall flow velocity distribution in Fig. 1 for a permeability value of 1.8×10^{-11} m^2. However, at some point, and at an unspecified loading, the axial PM distribution will become uniform, similar to that shown in Fig. 1 for a permeability value of 1.8×10^{-14} m^2. This result was also shown by Bensaid, Marchisio, Fino, Saracco, and Specchia [13]. Additionally, Yi [12] presented results for the radial distribution, after adding inlet and outlet connections to the substrate. Results from this work show a higher loading near the centerline of the substrate. The model never shows a uniform distribution in the radial direction. Konstandopoulos et al. [1] presented the modeled axial and radial PM distribution during a passive oxidation event. Results from their multichannel model showed that the PM was oxidized near the outlet of the substrate first. Then, as time progressed, the oxidation progressed from the outlet toward the inlet of the substrate. The passive oxidation resulted in a uniform axial distribution, with the PM loading at the inlet being only slightly higher than the outlet. The resulting radial distribution was nonuniform, with the periphery of the substrate having a higher PM loading than the centerline. The radial nonuniformity is likely caused by temperature and flow variations due to a suboptimal aftertreatment configuration. Kostoglou, Housiada, and Konstandopoulos [14] present multichannel simulation results that show how heat transfer, localized high temperature regions, and inlet nonuniformities affect the PM distribution during active regenerations. Although these modeling studies are outside the current scope of experimental

work, they do represent experimental work that needs to be completed in the future.

Although there are fewer experimental measurements of the PM distribution than the modeling studies, a few researchers have published results. The three following works studied the PM cake layer thickness in scaled down substrates. Koltsakis, Konstantinou, Haralampous, and Samaras [15] showed that when a substrate was loaded to 3.4 g/L, the PM cake layer thickness varied from 90 μm near the inlet, to 75 μm near the middle, and to 85 μm near the outlet of the substrate. As the overall loading increased to 8.2 g/L, the PM cake layer thickness was between 250 and 300 μm throughout the substrate. Bensaid, Marchisio, Russo, and Fino [16] conducted experimental work yielding similar results. One experiment had the minimum loading at 50 % of the axial length, which was 16–20 % lower than the PM loading near the inlet and outlet of the substrate. Another experiment, conducted at a lower overall loading, had the minimum loading at 35 % of the axial length. The PM loading at the minimum loading point was 33 % lower than at the outlet of the substrate, and the PM loading at the inlet was 13 % lower than at outlet of the substrate.

Pinturaud et al. [17] presented the axial PM distribution measurements for a scaled-down substrate. The axial PM distribution measured after PM loading in that study was similar to the wall flow velocity distribution shown in Fig. 1 for a permeability value of 1.8×10^{-12} m^2. Pinturaud et al. also performed an active regeneration on the scaled down substrate. After 41 % of the PM was oxidized, the general trend in the axial distribution was similar for the loading and active regeneration cases. This was the only work found that looked at the effect of active regenerations on the axial PM distribution.

Ranalli, Hossfeld, Kaiser, Schmidt, and Elfinger [18] found that the exhaust flow rate at which a substrate is loaded would affect the uniformity of the radial PM distribution. At 60 kg/h, a uniform PM distribution was found throughout the substrate for PM loadings from 0 to 9.3 g/L. However, at 320 kg/h, a nonuniform distribution was found after 5 g/L of PM was loaded. The authors used the flow rate of the exhaust through different areas of the substrate as a measurement of the uniformity, so the actual amount of variation in the PM loading was not quantified. Pinturaud et al. showed a similar result for PM loading in reference [17]. Pinturaud et al. [17] also showed that a uniform radial distribution existed after an active regeneration.

Lastly, Ranalli, Klement, Hoehnen, and Rosenberger [19] showed that the uniformity of the flow through the substrate is improved by optimizing the geometry of the piping leading into the substrate. Stratakis and Stamatelos [20] showed that placing a DOC directly in front of the particulate filter would improve the uniformity of the flow entering the substrate. Thus, it was concluded that improving the uniformity of the radial flow at the inlet to a CPF will make the PM distribution more uniform in the radial direction.

Although the literature gives an assessment of the PM distribution, the data and models come from a wide range of test systems. Various substrate sizes and measurement methods have been used for the many studies conducted. This may lead to differences in the resulting data that cannot be explained. It also becomes difficult to draw conclusions from these studies and compare the various models.

The study described in this paper focuses on collecting data under a well-controlled, consistent manner for loading, passive oxidation, active regeneration, and post loading conditions. Full-size aftertreatment components are used, and the PM distribution is analyzed in a nondestructive manner, so the resulting data is more representative of actual conditions. This makes interpreting the data and changes in the PM distribution more consistent, and the data provide significant value for CPF model development and validation.

2 Experimental Setup

A 2007 Cummins ISL rated at 272 kW was used for the experiments conducted for this study. The specifications for the engine are given in Table 1. All experiments were completed using ultra-low sulfur diesel fuel (ULSD). The CPFs used in this study used model year 2010 substrates and were canned using specialized apparatus. The specifications of the DOCs and CPFs used in this study are given in Table 2. The specialized cans used with the CPF substrate opened like a clamshell and allowed the substrate to be removed from the can prior to measuring the PM distribution. After the PM distribution measurement was taken, the substrate would be

Table 1 Engine specifications

Model	Cummins ISL 272 kW (365 HP)
Year of manufacture	2007
Cylinders	Inline 6
Bore and stroke	114×144.5 mm
Displacement	8.9 L
Aspiration	Turbocharged
Aftercooling	Cummins charge air cooler
Turbocharger	Holset variable geometry turbine
Rated power	272 kW @ 2100 rpm
Peak torque	1695 Nm @ 1400 rpm
EGR system	Electronically controlled and cooled

placed back in the can, and testing could resume. An example of the removable can is shown in Fig. 2. Figure 2a shows the can in the open position. Figure 2b shows the substrate in the can, which is instrumented for testing.

A schematic of the engine test cell used to conduct the experiments is shown in Fig. 3. The exhaust from the engine can be routed through one of two paths. The first path, called out as the "baseline," bypasses the exhaust aftertreatment system. The second path, called the "trapline," passes the exhaust through the aftertreatment system. Having two exhaust paths allows a test to be started and stopped at exact moments, by allowing the engine to be warmed or cooled without running exhaust through the aftertreatment system. The engine was connected to a wet gap eddy current dynamometer, rated at 373 kW. Gaseous emissions were measured using two instruments, a Pierburg AMA 4000 and a V&F Analyse- und Messtechnik GmbH AirSense ion molecule reaction mass spectrometer (IMR-MS). A scanning mobility

Table 2 DOC and CPF specifications

	DOC	CPF
Model year	2010	2010
Material	Cordierite	Cordierite
Diameter (mm)	267	267
Length (mm)	102	305
Cell geometry	Square	Square
Total volume (L)	5.7	17.0
Cell density (cells/mm^2)	0.62	0.31
Cell width (mm)	1.17	1.49
Filtration area (m^2)	N/A	15.72
Open frontal area (mm^2)	47,520	19,243
Channel wall thickness (mm)	0.11	0.30
Wall density (g/cm^3)	1.2	1.2
Porosity	35 %	52 %
Mean pore size (μm)	N/A	13
Number of inlet cells	34,714	8653
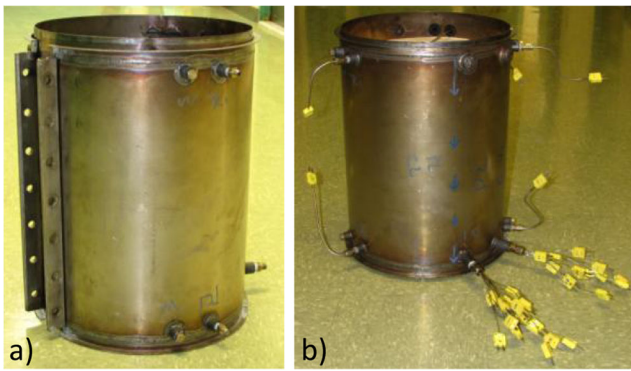
Fig. 2 Specialized can design. **a** Can in the open position. **b** Substrate in the can, which is instrumented for testing

particle sizer (SMPS) was used to measure particle size. The PM concentration in the exhaust was measured using a method developed by Michigan Technological University (MTU), which samples the hot exhaust and collects the PM on a 47-mm glass fiber filter. This filter is conditioned and weighed before and after testing, and the measured mass is divided by the standard volume of exhaust sampled to determine the PM concentration in mg/sm^3.

The PM distribution in the CPF was determined by scanning the substrate using an Advantest TAS7000 3D Imaging Analysis System, which uses terahertz waves. The TAS7000 detects changes in the transmitted terahertz wave and correlates the changes in a specific frequency spectrum to the amount of PM loaded in the substrate. The TAS7000 scans

the substrate in the 400-GHz to 4-THz frequency range [21]. For this study, the substrate was virtually divided into 125 axial sections, and each axial section was analyzed with a spatial resolution of a $4.5 \times 4.5 \times 2.4$-mm cuboid. The number of axial sections, and the spatial resolution, can be programmed into the TAS7000. A typical scan takes 6–20 h, depending on the desired spatial resolution. A substrate must be scanned twice for proper and accurate analysis. The first scan, referred to as a baseline scan, is of a clean substrate (no PM loading). The second scan is taken after a loading, passive oxidation, active regeneration, or post loading event. The difference in these two scans represents only the PM loading, as the base materials (substrate and washcoat) are removed from the analysis. Readers interested in the details of the TAS7000 that are beyond the scope of this paper should see references [5, 6].

The PM distribution is quantified using the average PM loading, the 95th percentile range (PR), and a uniformity index (UI). The 3D data from the TAS7000 were organized to allow for a thorough analysis. The data were grouped into 125 axial sections, four equal length axial segments, four equal area radial sections, 72 5° angular increments, and four quadrants. As stated previously, the number of axial sections used was determined during the scanning of the substrate. Figure 4 shows how an axial section was divided to achieve the four radial sections (given by the red lines and red text), the 72 5° angular increments (an example of one angular increment is given by the black lines), and the four quadrants

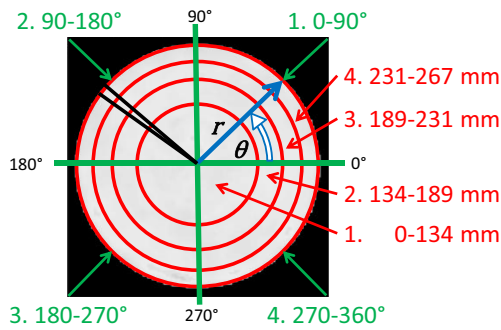**Fig. 3** Test cell schematic
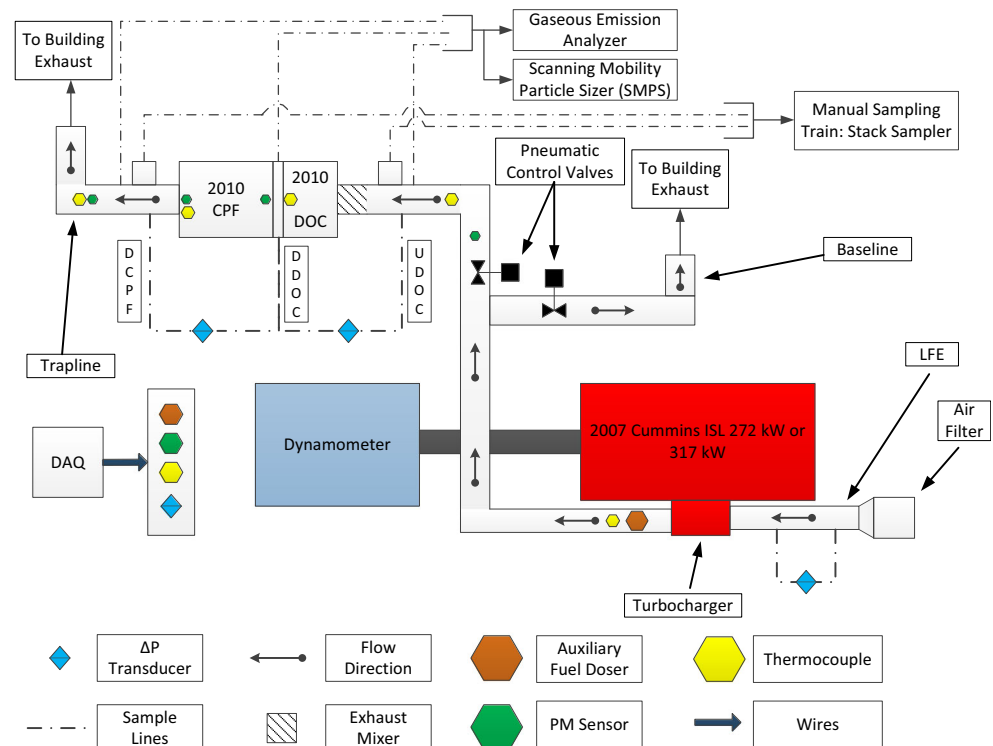
Fig. 4 Axial section divisions

(given by the green lines and green text). Figure 5 shows the axial segments, as a function of the normalized substrate length, Z^*. The value of Z^* is calculated using Eq. 1, where DFI is the distance from the inlet and OAL is the overall length of the substrate.

$$Z^* = \frac{DFI}{OAL} \tag{1}$$

This study used a UI to measure the amount of variation in the PM loading at the various analysis points in the substrate. An analysis point is defined as the area in one angular increment, one radial section, and one axial section. Defining the analysis point in this way allows for the resulting analysis to have directionality. These analysis points can be combined into analysis areas which represent the axial, radial, or angular direction, in axial sections, axial segments, or the entire substrate. The UI is calculated for a specific region, using the data in the analysis points and analysis areas. The UI was calculated using Eq. 2.

$$UI = 1 - \left(\frac{\sigma}{\overline{w}} \right) \tag{2}$$

In Eq. 2, σ is the standard deviation and $\overline{w}$ is the PM loading in the substrate at the completion of the loading portion of the test and prior to any oxidation event. The value of $\overline{w}$ was set to the total PM loading, in grams per liter, in the substrate at th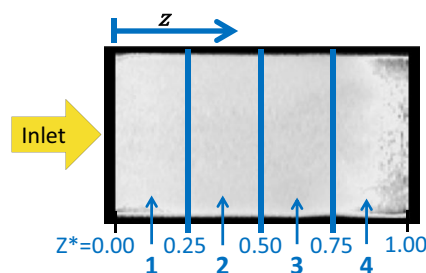e completion of the loading portion of the test to allow for easier comparison of the loading, passive oxidation, active regeneration, and post loading experiments. Sensitivity analysis showed that if the value of $\overline{w}$ varied by more than ± 0.8 g/L, the UI would vary by more than ± 4 %. Since the PM loading in the substrate at each individual scan varied from 1 to 5 g/L, it would be difficult to compare the UI values that resulted from different test conditions unless this sensitivity could be factored into the comparison. The PM loading in the substrate at the completion of the loading portion of the tests was around 3 g/L for all of the tests conducted, with the exception of two tests that were loaded to 5 g/L, enabling a better comparison of the different test conditions. The equation used to calculate σ is given as Eq. 3.

$$\sigma = \sqrt{\frac{\sum_{j=1}^{n_s} \left[\sum_{i=1}^{n} \left(w_i - \overline{w_l} \right)^2 \right]_j}{n_t}} \tag{3}$$

In Eq. 3, w_i is the PM loading in one analysis point in one analysis area, $\overline{w_l}$ is the average PM loading in one analysis area, n is the number of analysis points in each analysis area, n_s is the number of analysis areas being used in the calculation, and n_t is the total number of analysis points. The equation used to calculate n_t is given as Eq. 4.

$$n_t = (n)(n_s) \tag{4}$$

The use of the double summation in the calculation of σ allows for 3D analysis of the PM distribution, since both the number of analysis areas and analysis points can be changed. The double summation also allows for directionality to be maintained, since each analysis point is compared to an average value in a discrete direction. Therefore, a large area can be analyzed without taking the average value over a large area and decreasing the sensitivity of the analysis. An axial UI is always calculated using the average PM loading in the entire substrate, for either one radial section or as a whole, for the value of $\overline{w_l}$. A radial UI is always calculated using the average PM loading in one angular increment for the value of $\overline{w_l}$, regardless of the analysis area. An angular UI is always calculated using the average PM loading in one radial section as the value for $\overline{w_l}$, regardless of the analysis area. For the purposes of this work, a distribution will be described as uniform if the UI is greater than or equal to 0.94. Readers interested in more details of the analysis method should go to references [6, 7].

3 Experimental Plan

The experimental plan for phase 2 was designed to expand upon the data collected during phase 1 and to develop an understanding of how loading, passive oxidation, active

Fig. 5 Axial segment divisions

38

Emiss. Control Sci. Technol. (2015) 1:32–48
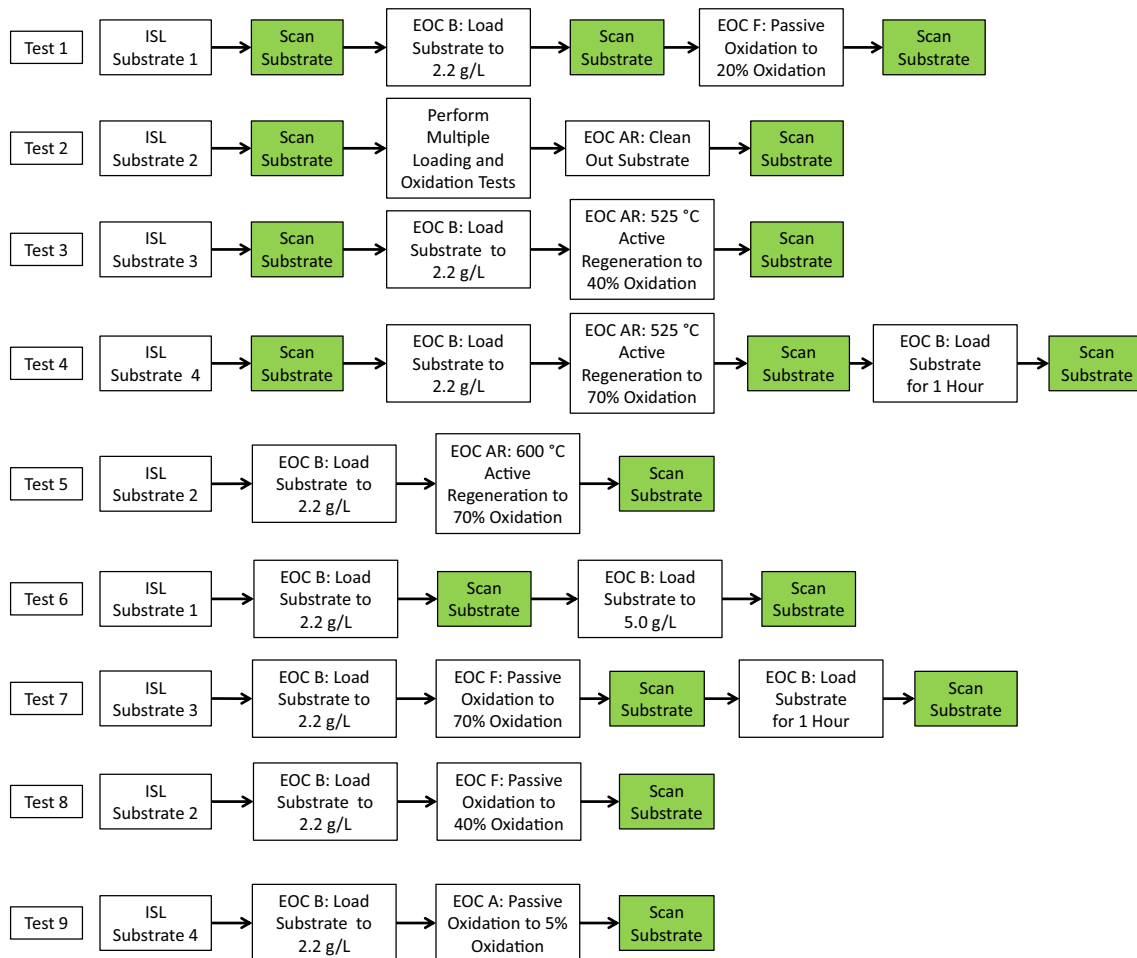
Fig. 6 Phase 2 experimental plan

regeneration, and post loading affect the PM distribution in the substrate. Details of phase 1 are presented in reference [6]. The developed test plan for phase 2 is shown in Fig. 6. Seventeen substrate scans were taken during phase 2. Of the 17 scans, four were baseline scans, three were loading scans, four were passive oxidation scans, four were active regeneration scans, and two were post loading scans. For the purposes of this paper, post loading is defined as PM loading that occurs after a

passive oxidation or active regeneration is performed on a substrate.

The engine operating conditions (EOCs) used during this study are given in Table 3. The EOCs and the test procedures were chosen as such in order to replicate passive oxidation and active regeneration experiments conducted by Hutton, Johnson, Naber, and Keith [22]; Shiel, Naber, Johnson, and Hutton [23]; and Pidgeon, Johnson, and Naber [24] and to gather

Table 3 Phase 2 engine operating conditions (EOCs)

EOC	Speed (rpm)	Load (Nm)	Percent of full load (%)	CPF space velocity (1 k/h)	Average CPF temp (°C)	O_2 conc. into CPF (%)	Engine out PM conc. (mg/scm)	NO_x conc. into CPF (ppm)	NO_x/PM ratio
B	2100	200	12	212	266	13.7	21.5	88	8
A	1200	280	17	89	256	12.5	5.8	283	89
F	1290	550	32	151	350	8.7	8.1	180	44
AR	1400	460	27	145	317	7.3	19.0	126	13

The space velocity was calculated by dividing the actual volumetric exhaust flow rate, in m^3/h, by the total substrate volume, in m^3. The actual volumetric flow rate of exhaust was calculated by dividing the exhaust mass flow rate, in kg/h, by the standard exhaust gas density, 1.18 kg/m^3, and then using the ideal gas equation to correct from the standard to the actual pressure and temperature. The temperature used was the average CPF temperature

more data for a one-dimensional CPF model being developed by Premchand, Surenahalli, and Johnson [25]. The one-dimensional model used the data from Shiel et al. [23] and Pidgeon et al. [24], to calibrate the different parameters to simulate the experimental results. The PM distribution data were one of the last pieces of information required for a better understanding of the results of the one-dimensional CPF model. The originally developed experimental procedure was modified to enable PM distribution measurements. The Appendix provides the overall procedure used to conduct the experiments.

4 Experimental Results

The study focused on developing an understanding of the PM distribution in a CPF after loading, passive oxidation, active regeneration, and post loading conditions. This section will present the results of each one of those conditions. The PM distribution results will also be summarized.

4.1 Loading Experimental Results

The axial PM distributions for the three loading experiments are shown in Fig. 7. The substrates were loaded to 3 and 5 g/L for these three tests. All loading experiments used EOC B, described in Table 3, as the loading condition. The overall trends for the 3 g/L experiments, tests 1 and 6, are similar. Test 1 had PM loadings that were 8 and 10 % higher than the calculated substrate average in axial segments 1 and 4, respectively. Axial segments 2 and 3 had PM loadings that were 5 to 11 % lower than the calculated substrate average. The substrate used for this experiment had not been previously tested; therefore, this PM distribution result represents the expected PM distribution after the loading of a clean substrate. The substrate used for test 6 had

been tested previously and was then cleaned out prior to test 6. The substrate was cleaned out using an active regeneration, which had exhaust temperatures near 600 °C, and was run until the pressure drop across the substrate was minimized and constant. The resulting PM distribution for test 6 was different than test 1, with axial segments 1–3 having PM loadings that were −3 to 0 % different than the calculated substrate average. Axial segment 4 had a PM loading that was 6 % higher than the calculated substrate average. The engine condition used to load the substrate for tests 1 and 6 was identical, so any change in the PM distribution was likely caused by artifacts of the previous loading on the substrate used for test 6. The artifacts may have changed the wall flow velocity distribution, which would have changed the PM loading distribution.

After the first loading scan from test 6 was taken, the substrate was loaded to 5.18 g/L, starting from the previous 2.81 g/L. The axial PM distribution is shown to change in Fig. 7 between test 6 and test 6 second loading. For test 6 second loading, axial segments 1–3 had PM loadings that were 2 to 6 % lower than the calculated average PM loading. This is similar to the distribution found for test 6. However, for axial segment 4, the PM loading was 13 % higher than the calculated substrate average. The increase in the loading near the outlet of the substrate was likely caused by a change in the wall flow velocity distribution. As shown in Fig. 1, the wall flow velocity profile is affected by permeability of the substrate and PM cake layer. The wall flow velocity profile is also affected by the exhaust flow rate. The exhaust flow rate did not change significantly between the two tests. Therefore, the permeability of the PM cake layer and the substrate wall would have to change as the PM loading increased in order to produce a different PM distribution trend. Additional data from these experiments are shown in Table 4.

Fig. 7 Axial PM distributions after loading
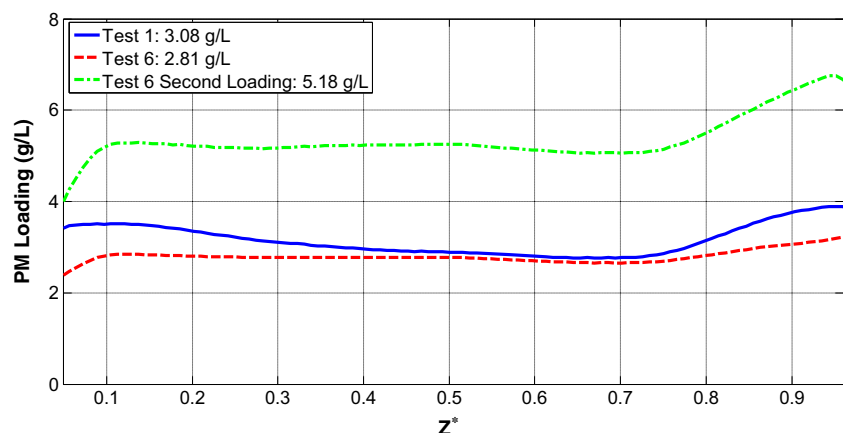
Table 4 PM distribution data summary for the loading experiments. The top row for each test contains the directional UI. Comments for each test are in the following row(s)

| Test	Axial distribution	Radial distribution	Angular distribution
Test 1—3.08 g/L	0.90	0.96	0.97
	•Axial segment 1—8 % higher •Axial segment 2—5 % lower •Axial segment 3—11 % lower •Axial segment 4—10 % higher	•All quadrants are uniform	•All radial sections are uniform
Test 6—2.81 g/L	0.94	0.97	0.97
	•Axial segment 1—2 % lower •Axial segment 2—0 % different •Axial segment 3—3 % lower •Axial segment 4—6 % higher	•All quadrants are uniform	•All radial sections are uniform
Test 6 second loading—5.18 g/L	0.89	0.95	0.95
	•Axial segment 1—6 % lower •Axial segment 2—2 % lower •Axial segment 3—4 % lower •Axial segment 4—13 % higher	•Quadrants 1 and 2 in axial segment 4 are non-uniform	•Radial sections 2 and 3 in axial segment 4 are non-uniform

The measured axial distribution was compared to a one-dimensional model developed by Premchand [26], and the result is shown in Fig. 8. Overall, the data from the model and the experiment have similar trends. Both show an increase in the PM loading near the inlet and outlet of the substrate, with a minimum occurring near the middle of the substrate. For the experimental data, that minimum value occurred at around 70 % of the axial length, and for the model, the minimum value occurred at around 40 % of the axial length. The modeled uses the wall flow velocity profile, which is calculated in the model, to predict the PM distribution [25, 26]. Although the reason for the differences in the trends is unknown, approximations in the model and model calibration could be part of the cause.

The radial and angular PM distributions were uniform for all of the loading experiments conducted. However, the UI for the axial PM distribution was found to vary based on the PM loading in the substrate. Figure 9 shows the axial UI as a function of the PM loading in the substrate. Test 6, which had a PM loading of 2.81 g/L, was the only test to have a uniform axial PM distribution. As the PM loading increased above 3 g/L, the axial UI dropped below 0.94, which is the threshold for a uniform distribution. This indicates that

Fig. 8 Comparison of experimentally measured to modeled axial PM distribution [26]. Reprinted with permission from Kiran Premchand's doctoral dissertation
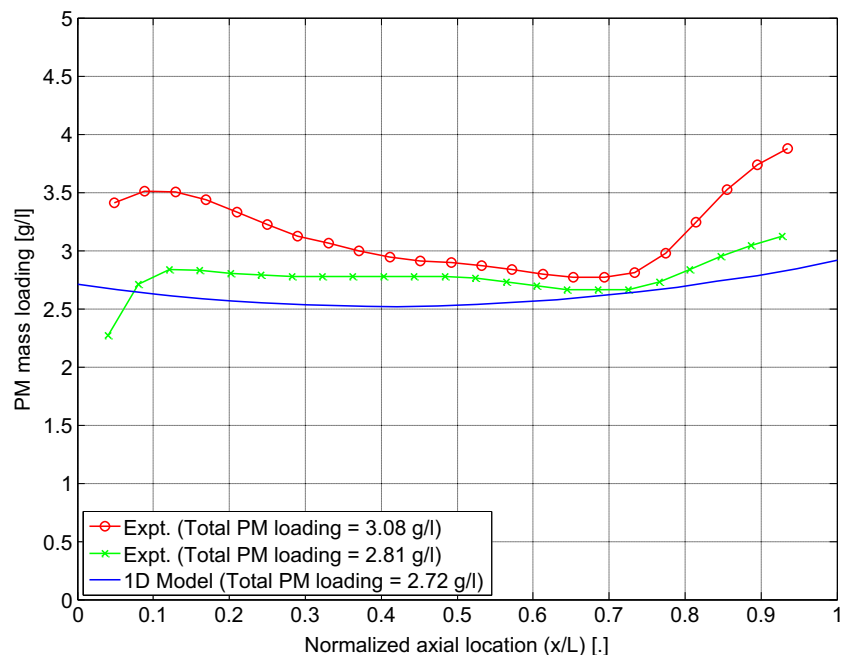
Fig. 9 Axial UI after PM loading
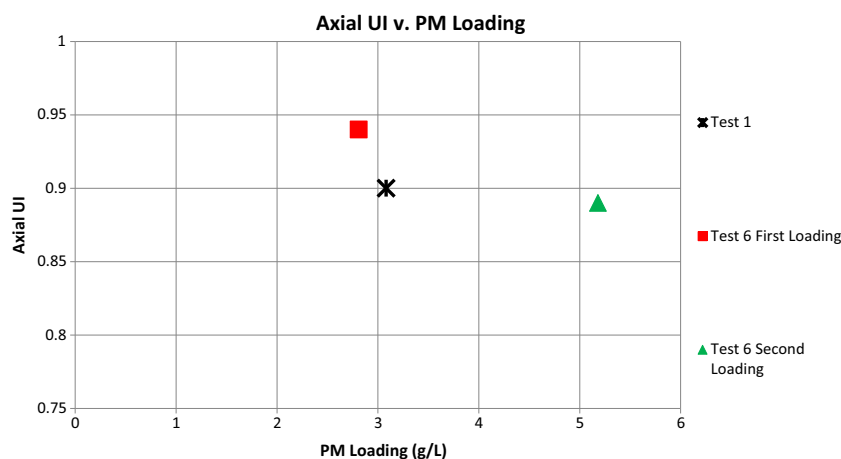
a PM loading below 3 g/L may be required to maintain a uniform axial PM distribution during substrate loading.

4.2 Passive Oxidation Experimental Results

The axial PM distributions measured for the four passive oxidation experiments are shown in Fig. 10. The axial distributions that were measured after passive oxidations show a trend similar to what was found after loading. The EOC used for tests 1, 7, and 8 was EOC F, described in Table 3. Test 9 used EOC A, also described in Table 3. The axial PM distribution after the passive oxidation in test 1, which oxidized 22 % of the available PM, had PM loadings in axial segments 1 and 4 that were 0 and 16 % higher than the calculated substrate average, respectively. Axial segments 2 and 3 had PM loadings that were 6 to 8 % lower than the calculated substrate average, respectively. The axial PM distribution after loading for test 1 had a similar distribution, with axial segments 1 and 4 having PM loadings that were 8 and 10 % higher than the calculated substrate average

and axial segments 2 and 3 having PM loadings that were 5 to 11 % lower than the calculated substrate average. The data indicate that more PM was oxidized near the inlet of the substrate. The passive oxidation portion of test 1 was completed directly after the loading scan was taken from test 1.

The axial PM distribution measured after the passive oxidation from test 7, where 65 % of the available PM was oxidized, had a different trend than what was found after the passive oxidation from test 1. Axial segments 1–3 had PM loadings that were between 2 and 4 % lower than the calculated substrate average. Axial segment 4 had a PM loading that was 10 % higher than the calculated substrate average. The difference in the PM distributions measured after the passive oxidation portions of tests 1 and 7 could be caused by the expected PM distribution after loading. The substrate used for test 7 had been previously used for testing. Therefore, the expected distribution after the loading portion of test 7 would be similar to the loading distribution measured for test 6. For test 6, axial segments 1–3 had PM loadings that were 0 to 3 % lower than the calculated substrate average and axial

Fig. 10 Axial PM distributions after passive oxidation. The numbers after test indicate percent oxidized and average substrate temperature
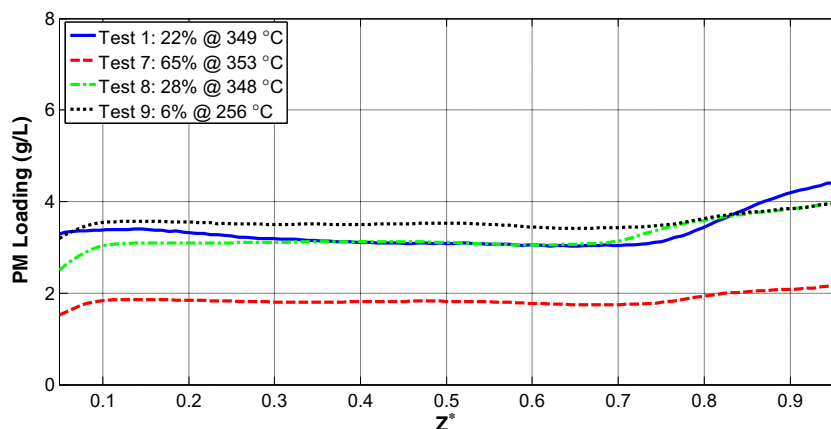
segment 4 had a PM loading that was 6 % higher than the calculated substrate average. This distribution is similar to what was found for test 7. The data show that less PM was oxidized near the outlet of the substrate, as the PM loading in axial segment 4 increased from being approximately 6 % higher than the calculated substrate average to being 10 % higher than the calculated substrate average. The PM loadings in axial segments 1–3 were similar for the loading scan of test 6 and the passive oxidation scan of test 7.

The measured axial PM distribution from test 8, where 28 % of the available PM was oxidized, was different than the axial PM distributions measured for tests 1 and 7. Axial segments 1–3 had PM loadings that were 3 to 8 % lower than the calculated substrate average. Axial segment 4 had a PM loading that was 16 % higher than the calculated substrate average. This result shows that passive oxidation removes more PM from the inlet area of the substrate initially, since the PM loading near the outlet of the substrate for test 8 is higher than the PM loading near the outlet for tests 1 and 7. Axial segments 1–3 had similar PM loadings for tests 1, 7, and 8.

The axial PM distribution that was measured for test 9, where 6 % of the available PM mass was oxidized, was similar to the result for test 7. The PM loadings in axial segments 1–3 were 1 to 3 % lower than the calculated substrate average. Axial segment 4 had a PM loading that was 6 % higher than the substrate average. Test 9 used EOC A, instead of EOC F, as test 7 did. Both EOCs are described in detail in Table 3. The space

velocity and average substrate temperature for EOC A was 41 and 27 % lower, respectively, than EOC F. This indicates that the space velocity and average substrate temperature did not have a significant effect on the axial PM distribution for these tests. Additional data for the passive oxidation experiments are found in Table 5.
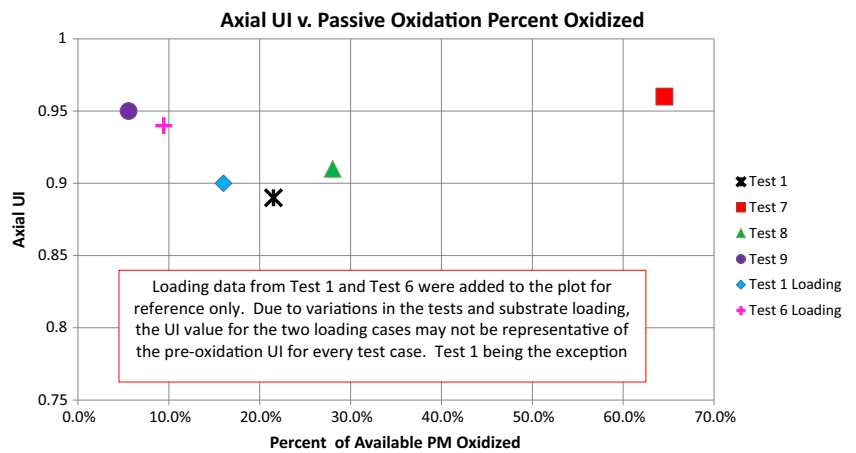
In general, the difference between the PM loading in axial segment 4 and the substrate average was greater for the passive oxidation experiments than the loading experiments. This is possibly explained by particle physics. Sappok, Wang, Wang, Kamp, and Wong [27] discuss how PM moves in a substrate channel during passive oxidation and active regeneration events. Their work shows that during the PM oxidation process, PM can become re-entrained in the flow and transported toward the outlet of the substrate. During passive oxidation events, the PM reaction rate would remain nearly constant in the axial direction, from the inlet to the outlet of the substrate, as there are no large axial temperature variations. Therefore, the PM loading near the outlet of the substrate would increase, since there would be no increase in the PM reaction rate to remove the re-entrained and re-deposited PM.

The axial UIs for the passive oxidation experiments are shown in Fig. 11 as a function of the amount of PM oxidized. The radial and angular UIs are not shown since they were found to be uniform for all experiments. In Fig. 11, the axial PM distribution was uniform when 6 and 65 % of the available PM were oxidized. When

Table 5 PM distribution data summary for the passive oxidation experiments. The top row for each test contains the directional UI. Comments for each test are in the following row(s)

Test	Axial distribution	Radial distribution	Angular distribution
Test 1—22 % oxidized @ 349 °C	0.89	0.97	0.98
	•Axial segment 1—0 % different •Axial segment 2—6 % lower •Axial segment 3—8 % lower •Axial segment 4—16 % higher	•All quadrants are uniform	•All radial sections are uniform
Test 7—65 % oxidized @ 353 °C	0.96	0.98	0.99
	•Axial segment 1—3 % lower •Axial segment 2—2 % lower •Axial segment 3—4 % lower •Axial segment 4—10 % higher	•All quadrants are uniform	•All radial sections are uniform
Test 8—28 % oxidized @ 348 °C	0.91	0.97	0.98
	•Axial segment 1—8 % lower •Axial segment 2—3 % lower •Axial segment 3—3 % lower •Axial segment 4—16 % higher	•All quadrants are uniform	•All radial sections are uniform
Test 9—6 % oxidized @ 256 °C	0.95	0.97	0.98
	•Axial segment 1—2 % lower •Axial segment 2—1 % lower •Axial segment 3—3 % lower •Axial segment 4—6 % higher	•All quadrants are uniform	•All radial sections are uniform

Axial UI v. Passive Oxidation Percent Oxidized

Loading data from Test 1 and Test 6 were added to the plot for reference only. Due to variations in the tests and substrate loading, the UI value for the two loading cases may not be representative of the pre-oxidation UI for every test case. Test 1 being the exception

Legend:
- ✖ Test 1
- ■ Test 7
- ▲ Test 8
- ● Test 9
- ◆ Test 1 Loading
- ✚ Test 6 Loading

more than 6 % and less than 65 % of the available PM were oxidized during a passive oxidation event, a non-uniform axial distribution was found.

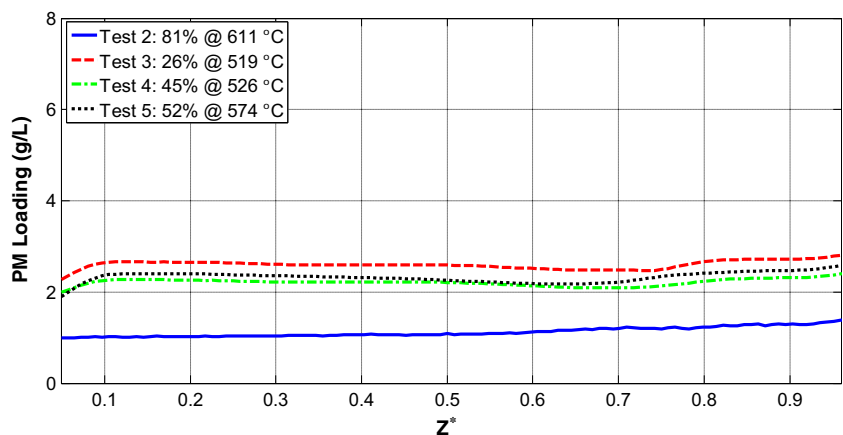### 4.3 Active Regeneration Experimental Results

Four active regeneration experiments were conducted as part of this study, with the axial PM distributions for the four substrate scans shown in Fig. 12. All active regeneration experiments used EOC AR, described in Table 3, and in-cylinder fuel dosing to complete the active regeneration. The CPF inlet temperature was varied from 525 to 600 °C, depending on the test being conducted. The active regeneration experiments resulted in an axial PM distribution trend that was similar to what was found after PM loading experiments.

Test 2 was a substrate cleanout at 611 °C where 81 % of the available PM was oxidized. The PM loading in the substrate prior to the cleanout was 4.88 g/L. This was the only active regeneration experiment with a PM loading near 5 g/L. The other active regeneration experiments were performed on a substrate loaded to approximately 3 g/L. The PM loading for test 2 increases from being 9 % lower than the calculated substrate average in axial segment 1 to being 14 % higher than the calculated substrate average in axial segment 4. Axial segments 2 and 3 had PM loadings that were −6 and 2 % different than the calculated average substrate loading. The slight increase is likely due to ash deposits in the substrate. The substrate used for test 2 was used for an additional 70 h of engine run time prior to the cleanout taking place. It was shown in reference [7] that 70 h of operation is long enough to deposit 13 g (0.76 g/L) of ash in a CPF. During the experiment, the rate of change in the pressure drop during the last 5 min of the cleanout was 6 Pa/min. This indicates that the pressure drop was stabilizing prior to the experiment being stopped and a majority of the carbonaceous PM was oxidized. Therefore, the resulting trend in the line may represent an ash distribution in the substrate.

Phase 2 tests 3–5 all have similar axial PM distributions. These tests oxidized 26, 45, and 52 % of the available PM at 519, 525, and 574 °C, respectively. For test 3, axial sections 1–3 had PM loadings that were −3 to 0 % different than the calculated substrate average. Axial

Legend:
- Test 2: 81% @ 611 °C
- Test 3: 26% @ 519 °C
- Test 4: 45% @ 526 °C
- Test 5: 52% @ 574 °C

Table 6 PM distribution data summary for the active regeneration experiments. The top row for each test contains the directional UI. Comments for each test are in the following row(s)

| Test	Axial distribution	Radial distribution	Angular distribution
Test 2—81 % oxidized @ 611 °C	0.97	0.99	0.98
	•Axial segment 1—9 % lower •Axial segment 2—6 % lower •Axial segment 3—2 % higher •Axial segment 4—14 % higher	•All quadrants are uniform	•All radial sections are uniform
Test 3—26 % oxidized @ 519 °C	0.96	0.97	0.97
	•Axial segment 1—0 % different •Axial segment 2—0 % different •Axial segment 3—3 % lower •Axial segment 4—4 % higher	•All quadrants are uniform	•All radial sections are uniform
Test 4—45 % oxidized @ 526 °C	0.97	0.98	0.98
	•Axial segment 1—0 % different •Axial segment 2—0 % different •Axial segment 3—4 % lower •Axial segment 4—3 % higher	•All quadrants are uniform	•All radial sections are uniform
Test 5—52 % oxidized @ 574 °C	0.96	0.98	0.98
	•Axial segment 1—1 % lower •Axial segment 2—0 % different •Axial segment 3—4 % lower •Axial segment 4—6 % higher	•All quadrants are uniform	•All radial sections are uniform

section 4 from test 3 was 4 % higher than the calculated substrate average. This is similar to what was found for the loading scan from test 6. Axial sections 1–3 for test 4 had PM loadings that were −4 to 0 % different than the calculated substrate average, and axial section 4 was 3 % higher than the calculated substrate average. Test 5 produced similar results as well, with axial sections 1–3 having PM loadings that were −4 to 0 % different than the calculated substrate average, and axial section 4 was 6 % higher than the calculated substrate average. This shows that the average substrate temperature during the active regeneration, and the amount of PM that was oxidized, did not have an impact on the axial PM distribution

for these experiments. Additional data for the active regeneration experiments are given in Table 6.

The difference between the PM loading in axial segment 4 and the substrate average is not significantly different than what was found for the loading experiments. Sappok et al. [27] discuss that active regenerations can cause particle re-entrainment similar to passive oxidations, possibly causing more particles to move toward the outlet of the substrate. However, during active regenerations, the temperature near the outlet of the substrate can be 25 °C higher than the inlet of the substrate, as shown in reference [7]. For an active regeneration with a target temperature of 600 °C, the 25 °C

Fig. 13 Axial UI after active regeneration
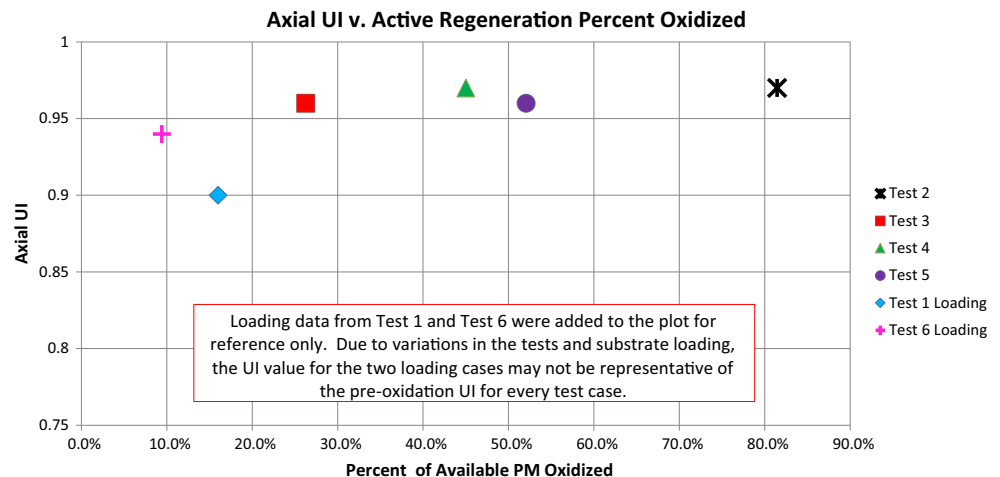
Fig. 14 Axial PM distributions
after post loading following active
regeneration (test 4) and passive
oxidation (test 7) tests

The legend reads:
Test 4: 2.22-3.47 g/L & UI=0.84
Test 7: 1.85-2.99 g/L & UI=0.95
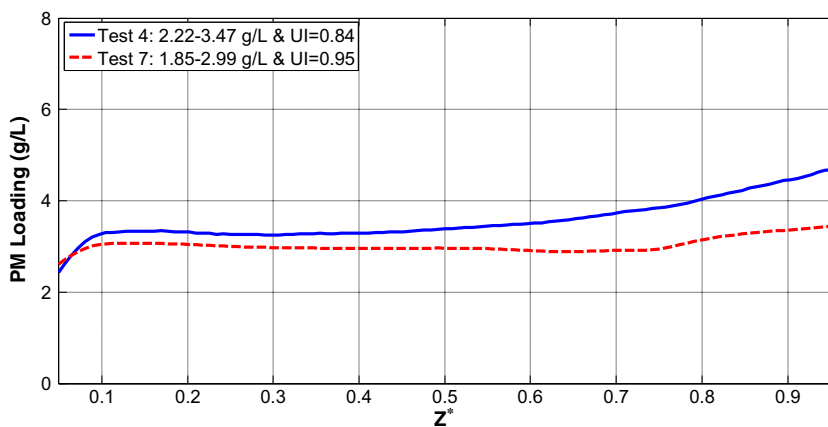
increase near the outlet can increase the PM reaction rate by 66 % [7]. These phenomena are counteracting, where the increased reaction rate could be oxidizing the excess PM that would be re-deposited near the outlet of the substrate.

Figure 13 shows the axial UI for the four active regeneration experiments versus the amount of PM oxidized. The axial UI was above 0.94 for all active regeneration experiments. The radial and angular UIs are not shown since they were uniform for all experiments as well. This indicates that the active regenerations did not result in nonuniform PM distribution.

4.4 Post Loading Experimental Results

The final section of results covers the post loading results. Post loading is defined as the loading that occurs after a passive oxidation or active regeneration event. Two post loading experiments were conducted, one after a passive oxidation and one after an active regeneration. Both post loading experiments used EOC B, described in Table 3, as the loading condition. The axial PM

distributions for both experiments are shown in Fig. 14. The substrate scan from test 4 shows the result of post loading after an active regeneration. Test 4 was a 526 °C active regeneration that oxidized 45 % of the available PM. The substrate scan from test 7 shows the result of post loading after a passive oxidation. Test 7 was a passive oxidation at EOC F that oxidized 65 % of the available PM. Results for the radial and angular distribution are not discussed because both experiments had uniform radial and angular distributions. The axial UI for the post loading portion of test 4 was 0.84, and the axial UI for test 7 was 0.95. The two post loadings resulted in a similar amount of PM being added to the substrate. The post loading for tests 4 and 7 increased the average PM loading by 56 and 62 %, respectively. Since the post loading increased the PM loading in the substrate by a similar amount, the decrease in the uniformity of the axial PM distribution was likely caused by the active regeneration.

The axial PM distribution found for the post loading scan from test 4, which was after an active regeneration, is unlike any other axial PM distribution, with the exception of test 2, which was a 611 °C active regeneration that oxidized 81 % of

Table 7 PM distribution data summary for the post loading experiments. The top row for each test contains the directional UI. Comments for each test are in the following row(s)

Test	Axial distribution	Radial distribution	Angular distribution
Test 4—2.22 to 3.47 g/L Increase of 1.25 g/L	0.84	0.95	0.95
	•Axial segment 1—11 % lower •Axial segment 2—8 % lower •Axial segment 3—1 % higher •Axial segment 4—20 % higher	•Non-uniform distributions in °Quadrant 2 in axial segment 1 °Quadrant 2 in axial segment 3 °Quadrants 1, 2, and 4 in axial segment 4	•Radial sections 3 and 4 had non-uniform distributions in axial segments 1 and 4
Test 7—1.85 to 2.99 g/L Increase of 1.14 g/L	0.95	0.97	0.98
	•Axial segment 1—2 % lower •Axial segment 2—2 % lower •Axial segment 3—3 % lower •Axial segment 4—8 % higher	•All quadrants are uniform	•All radial sections are uniform

the available PM. For test 4, axial segments 1–3 had PM loadings that were −11 to 1 % different than the calculated substrate average. Axial segment 4 had a PM loading that was 20 % higher than the calculated substrate average. After the active regeneration that was performed during test 4, the PM loadings in axial segments 1–4 were −4 to 3 % different than the substrate average. This indicates that the wall flow velocity distribution changed after the active regeneration, causing the axial PM distribution to change. This is likely caused by a change in the permeability of the substrate wall and PM cake layer. Additional data for the post loading experiments are given in Table 7.

The axial PM distribution for the post loading scan from test 7, which was after a passive oxidation event, is similar to the axial PM distribution found after the passive oxidation experiments. Axial sections 1–3 had PM loadings that were −3 to −2 % different than the calculated substrate average. Axial section 4 had a PM loading that was 8 % higher than the substrate average. The similarity in the axial PM distributions from the post loading scan of test 7 and the passive oxidation scan of test 7 indicates that the passive oxidation event did not alter the wall flow velocity distribution and, thus, the permeability of the substrate wall and PM cake layer.

5 Summary and Conclusions

The axial wall flow velocity is one of the main factors in determining the axial PM distribution, due to the size of the particles in the exhaust. The models developed show PM distributions that are similar to the axial wall flow velocity. Other experiments have been conducted that show a correlation between the axial wall flow velocity and the PM distribution. The experimental work for this study was conducted using a 2007 Cummins ISL diesel engine. The substrates were scanned using an Advantest TAS7000 3D Imaging Analysis System. The results from three loading, four passive oxidation, four active regeneration, and two post loading tests were presented. Table 4 presents the results from the three loading experiments. The results from the four passive oxidation experiments are shown in Table 5. Table 6 presents a summary of the four active regeneration experiments. The two post loading experiments are summarized in Table 7.

The conclusions from this work are as follows.

For loading experiments:

- The axial PM distribution after loading has a similar trend to the simulated axial wall flow velocity distribution.
- The axial UI decreases as the PM loading in the substrate increases. The radial and angular UI values were greater than 0.94 for all cases and showed no trends.

For passive oxidation experiments:

- The axial PM distributions from the passive oxidation experiments were similar to the axial PM distributions found during the loading experiments; however, less PM was oxidized near the outlet of the substrate.
- The axial UI decreases when more than 6 % and less than 65 % of the available PM are oxidized. The radial and angular UI values were greater than 0.94 for all cases and showed no trends.

For active regeneration experiments:

- The axial PM distributions from the active regeneration experiments were similar to the axial PM distributions found during the loading experiments.
- The axial, radial, and angular UI was greater than 0.94 for all active regeneration experiments and thus considered uniform.

For post loading experiments:

- Post loading after a passive oxidation event resulted in an axial PM distribution that was similar to the other loading and passive oxidation axial PM distributions.
- Post loading after an active regeneration resulted in a different axial PM distribution than the loading, passive oxidation, and active regeneration axial PM distributions. This is likely caused by a change in the permeability of the substrate wall and PM cake layer.
- The axial UI was greater than 0.94 for the post loading after a passive oxidation, but less than 0.94 for the post loading after the active regeneration. The radial and angular UI values were greater than 0.94 and showed no trend.

legal liability or responsibility for the accuracy, completeness, or usefulness of any information, apparatus, product, or process disclosed, or represents that its use would not infringe privately owned rights. Reference herein to any specific commercial product, process, or service by trade name, trademark, manufacturer, or otherwise does not necessarily constitute or imply its endorsement, recommendation, or favoring by the US Government or any agency thereof. The views and opinions of authors expressed herein do not necessarily state or reflect those of the US Government or any agency thereof.

Appendix. Test procedures

The test procedure for preparing, testing, and scanning the CPFs for loading, passive oxidation, active regeneration, and post loading is given in Fig. 15.

The multiple steps allow a test to be customized depending on the desired outcome of the test.
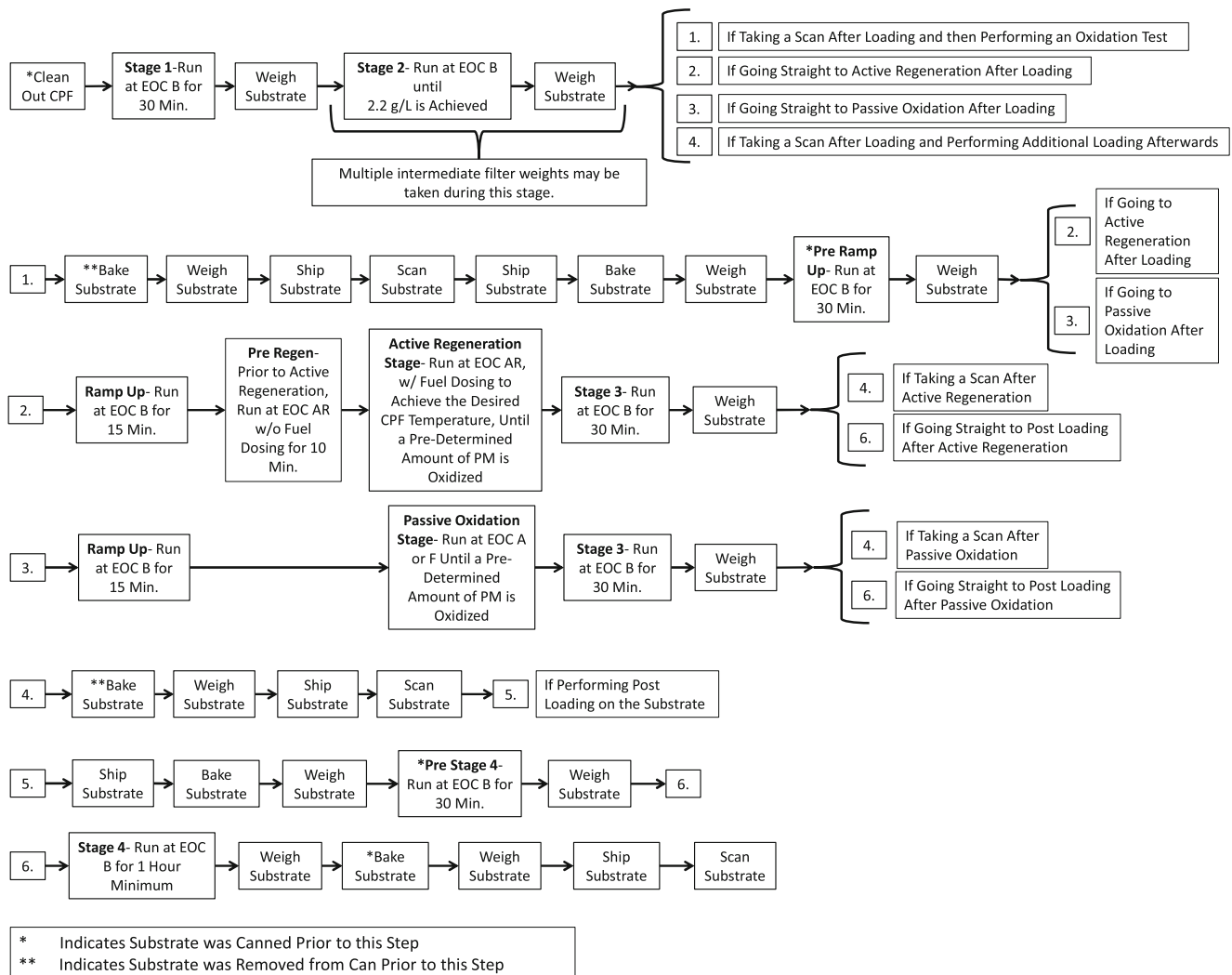
Fig. 15 Complete test procedure used for the various experiments

References

1. Konstandopoulos, A., Kostoglou, M., and Housiada, P., Spatial non-uniformities in diesel particulate trap regeneration, SAE Technical Paper 2001-01-0908, 2001, doi:10.4271/2001-01-0908

2. Sandhuis, J., Finney, C., Toops, T., Partridge, W., Daw, C., and Fox, T., Nondestructive X-ray inspection of thermal damage soot and ash distributions in diesel particulate filters, SAE Technical Paper 2009-01-0289, 2009, doi:10.4271/2009-01-0289

3. Harvel, G., Chang, J., Ewing, D., Fanson, P., and Kakinohana, M., Measurement of multi-dimension soot distribution in diesel particulate filters by a dynamic neutron radiography, SAE Technical Paper 2009-01-1263, 2009, doi:10.4271/2009-01-1263

4. Harvel, G., Chang, J., Tung, A., Fanson, P., and Watanabe, M., Three-dimension deposited soot distribution measurement in silicon carbide diesel particulate filters by dynamic neutron radiography, SAE Technical Paper 2011-01-0599, 2011, doi:10.4271/2011-01-0599

5. Nishina, S., Takeuchi, K., Shinohara, M., Imamura, M., Shibata, M., Hashimoto, Y., and Watanabe, F., Novel nondestructive imaging analysis for catalyst washcoat loading and DPF soot distribution using terahertz wave computed tomography, SAE Technical Paper 2011-01-2064, 2011, doi:10.4271/2011-01-2064

6. Foley, R., Naber, J., Johnson, J., and Rogoski, L., Development of the methodology for quantifying the 3D PM distribution in a catalyzed particulate filter with a terahertz wave scanner, SAE Technical Paper 2014-01-1573, 2014, doi:10.4271/2014-01-1573

7. Foley, R., Experimental investigation into particulate matter distribution in catalyzed particulate filters using a 3D Terahertz wave scanner, Master's Thesis, Michigan Technological University, 2013

8. Konstandopoulos, A., and Johnson, J., Wall-flow diesel particulate filters—their pressure drop and collection efficiency, SAE Technical Paper 890405, 1989, doi:10.4271/890405

9. Ohara, E., Mizuno, Y., Miyairi, Y., Mizutani, T., Yuuki, K., Noguchi, Y., Hiramatsu, T., Makino, M., Takahashi, A., Sakai, H., Tanaka, M., Martin, A., Fujii, S., Busch, P., Toyoshima, T., Ito, T., Lappas, I., and Vogt, C., Filtration behavior of diesel particulate filters (1), SAE Technical Paper 2007-01-0921, 2007, doi:10.4271/2007-01-0921

10. Liu, Y., Gong, J., Fu, J., Cai, H., Long, G.: Nanoparticle motion trajectories and deposition in an inlet channel of wall-flow diesel particulate filter. J. Aerosol Sci. **40**(4), 307–323 (2009). doi:10.1016/j.jaerosci.2008.12.001

11. Piscaglia, F., Rutland, C., and Foster, D., Development of a CFD model to study the hydrodynamic characteristics and the soot deposition mechanism on the porous wall of a diesel particulate filter, SAE Technical Paper 2005-01-0963, 2005, doi:10.4271/2005-01-0963

12. Yi, Y., Simulating the soot loading in wall-flow DPF using a three-dimensional macroscopic model, SAE Technical Paper 2006-01-0264, 2006, doi:10.4271/2006-01-0264

13. Bensaid, S., Marchisio, D.L., Fino, D., Saracco, G., Specchia, V.: Modelling of diesel particulate filtration in wall-flow traps. Chem. Eng. J. **154**(1–3), 211–218 (2009). doi:10.1016/j.cej.2009.03.043

14. Kostoglou, M., Housiada, P., Konstandopoulos, A.: Multi-channel simulation of regeneration in honeycomb monolithic diesel particulate filters. Chem. Eng. Sci. **58**(14), 3273–3283 (2003). doi:10.1016/S0009-2509(03)00178-7

15. Koltsakis, G. C., Konstantinou, A., Haralampous, O. A., and Samaras, Z. C., Measurement and intra-layer modeling of soot density and permeability in wall-flow filters, SAE Technical Paper 2006-01-0261, 2006, doi:10.4271/2006-01-0261

16. Bensaid, S., Marchisio, D.L., Russo, N., Fino, D.: Experimental investigation of soot deposition in diesel particulate filters. Catal. Today **147**, 295–300 (2009). doi:10.1016/j.cattod.2009.07.039

17. Pinturaud, D., Charlet, A., Caillol, C., Higelin, P., Girot, P., Briot, A., Experimental study of DPF loading and incomplete regeneration, SAE Technical Paper 2007-24-0094, 2007, doi:10.4271/2007-24-0094

18. Ranalli, M., Hossfeld, C., Kaiser, R., Schmidt, S., and Elfinger, G., Soot loading distribution as a key factor for a reliable DPF system: an innovative development methodology, SAE Technical Paper 2002-01-2158, 2002, doi:10.4271/2002-01-2158

19. Ranalli, M., Klement, J., Hoehnen, M., and Rosenberger, R., Soot distribution in DPF systems. A simple and cost effective measurement method for series development, SAE Technical Paper 2004-01-1432, 2004, doi:10.4271/2004-01-1432.

20. Stratakis, G.A., Stamatelos, A.M.: Flow maldistribution measurements in wall-flow diesel filters. Proc. IME Part D: J. Automob. Eng. **218**(9), 995–1009 (2004). doi:10.1243/0954407041856854

21. Self, G., Advantest America, Inc, personal communication, Oct. 2012

22. Hutton, C., Johnson, J., Naber, J., Keith, J., Procedure development and experimental study of passive particulate matter oxidation in a diesel catalyzed particulate filter, SAE Technical Paper 2012-01-0851, 2012, doi:10.4271/2012-01-0851

23. Shiel, K., Naber, J., Johnson, J., Hutton, C., Catalyzed particulate filter passive oxidation study with ULSD and biodiesel blended fuel, SAE Technical Paper 2012-01-0837, 2012, doi:10.4271/2012-01-0837

24. Pidgeon, J., Johnson, J., Naber, J., An experimental investigation into particulate matter oxidation in a catalyzed particulate filter with biodiesel blends on an engine during active regeneration, SAE Technical Paper 2013-01-0521, 2013, doi:10.4271/2013-01-0521

25. Premchand, K., Surenahalli, H., and Johnson, J., Particulate matter and nitrogen oxides kinetics based on engine experimental data for a catalyzed diesel particulate filter, SAE Technical Paper 2014-01-1553, 2014, doi:10.4271/2014-01-1553

26. Premchand, K. C., Development of a n catalyzed diesel particulate filter model using engine experimental data for simulation of the performance and the oxidation of particulate matter and oxides of nitrogen during passive oxidation and active regeneration, Doctor of Philosophy, Michigan Technological University, 2013

27. Sappok, A., Wang, Y., Wang, R., Kamp, C., Wong, V., Theoretical and experimental analysis of ash accumulation and mobility in ceramic exhaust particulate filters and potential for improved ash management, SAE Int. J. Fuels Lubr. 7(2): 2014, doi:10.4271/2014-01-1517